

# Scalar Calibration for Broadband Phaseless Antenna Measurements Based on Indirect Off-Axis Holography

Ana Arboleya, Jaime Laviada and Fernando Las-Heras

**Abstract**—A scalar calibration method for broadband off-axis holography phaseless antenna characterization and diagnostics is presented in this manuscript. With the proposed method, the need of vector calibration, inherent to off-axis holography setups, is bypassed by means of an intermediate step in which a well known antenna, whose phase can be analytically modeled, is used to retrieve the phase of the reference antenna by applying the off-axis holography method twice. The method is specially suited for near-field characterization of high gain millimeter and submillimeter-wave antennas in which phase acquisition is a difficult task, requiring complex and expensive instrumentation and steady conditions. The phase of the field is retrieved at each point of the acquisition surface for a set of frequencies and, consequently, the technique can be applied independently of the acquisition geometry. Validation examples are presented in the W-band.

**Index Terms**—Amplitude-only, Antenna Measurement, Broadband, Diagnostics, Millimeter-wave, Off-axis Holography, Phaseless, Calibration.

## I. INTRODUCTION

Phase acquisition, especially at high frequency bands such as millimeter- (mm-) and submillimeter (submm-) wave bands, is a difficult task due to the high thermal stability and positioning accuracy requirements as well as the effect of errors such as cable flexing [1]. Thus, during the last years, phaseless techniques capable of retrieving the phase of the field from amplitude-only measurements are widespread.

Among phaseless techniques, indirect off-axis holography is one of the most employed methods for phase retrieval. It was coined by Gabor [2] and adapted to use an off-axis reference by Leith and Upatnieks [3] in the optics field and, later, adapted for antenna characterization in the microwave bands by Napier [4] and Bennett [5]. As an interferometric technique, indirect off-axis holography is based on the knowledge of a reference field (in amplitude and phase) which is used to record an interference pattern with the field of the antenna under test (AUT) allowing for the phase retrieval of the field of the AUT in the spatial domain [6]–[8]. Accuracy of these holographic techniques is limited by positioning errors and errors in the characterization of the reference field [6], [9] and also by the spectral overlap of the terms of the hologram, which can be controlled by resorting to synthesized wave holography [7], [8] or hybrid schemes [10].

The other main phase retrieval approach is based on iterative methods. Those methods rely on the spatial variation of the electric near-field (NF) with distance and therefore, require the amplitude acquisition in, at least, two different surfaces [11]–[13]. Then, the phase is retrieved in both surfaces after an iterative process. Iterative methods are popular because they involve minimum changes in the

setup. Nevertheless, it is well known that they can suffer from stagnation due to the employed non-linear solvers. In addition, they provide good results when the field variability between both acquisition surfaces is high and an appropriate first guess solution is chosen [12]. In contrast to iterative methods, in indirect off-axis holography there are no specific requirements about variability of the field and, therefore, the technique is able to provide good results with all types of antennas, specially when applied for phase retrieval of high gain antennas such as reflectors with low NF variability [6].

Recently, a new method based on indirect off-axis holography for phaseless characterization of broadband antennas has been published in [14]. This method is able to retrieve the phase independently at each point of the acquisition plane and, therefore, standard or enhanced sampling criteria [15] can be used. However, as for conventional off-axis holography techniques, the main drawback of this method is the need of knowing the phase of the reference antenna, making necessary to resort to vector calibration of the measurement system.

Several scalar calibration methods to bypass the need of characterizing the phase of the reference antenna are available for off-axis holography *imaging* techniques [16], [17]. Those methods are able to guess the exact position of the reference antenna by means of iterative processes, which search the best focused image. Then the phase of the reference signal can be analytically modeled if the reference antenna is a well-known and simple antenna. The aforementioned approach for imaging cannot be easily applied to antenna measurements despite a characterization of the reference antenna is also required. To the best authors' knowledge, the two only ways to characterize the reference antenna are: (a) by placing it far enough from the AUT, with the subsequent losses to convey the signal, so its radiation pattern can be approximated by a plane-wave or (b) by using an initial vector calibration. In general, it is clearly recommendable to avoid the latter strategy as it requires vector equipment and, also, because any change of the reference antenna (e.g., it could be required to illuminate different areas due to the use of different acquisition planes and distances, or the physical dimensions of the AUT could collide with the reference antenna making necessary to adjust the position of this one) would require a new vector calibration.

In this contribution, the complex field in the acquisition plane and the exact position of the reference antenna are retrieved by means of an additional step in which an auxiliary antenna, placed in a known position, is employed to create the interference pattern with the reference antenna. If the acquisition plane is illuminated by the main lobe of a simple auxiliary antenna, its phase can be analytically modeled yielding to a purely *scalar non-iterative technique*. This auxiliary antenna can be placed at a fix known position, e.g., taking advantage of the AUT feeding system. The retrieved phase of the field of the reference antenna is employed in the final setup to estimate the phase of the AUT by applying the broadband off-axis technique [14] a second time.

The herein presented method is applied to planar NF antenna measurements, although it can be applied similarly to other acquisition domains. Since the phase retrieval is done point by point, it is non-dependent on the acquisition geometry and conventional non-

Manuscript received Month day, 2017. This work was supported in part by the Ministerio de Ciencia e Innovación of Spain/FEDER under project PortEMVision-TEC2014-55290-JIN; by the Gobierno del Principado de Asturias through the PCTI/FEDER-FSE 2013-2017 under project GRUPIN14-114 and by Ayudas Fundación BBVA a Investigadores y Creadores Culturales.

Ana Arboleya is with the Departamento de Teoría de la Señal y las Comunicaciones y Sistemas Telemáticos y Computación, Universidad Rey Juan Carlos, Spain (e-mail: ana.arboleya@urjc.es). Jaime Laviada and Fernando Las-Heras are with the Departamento de Ingeniería Eléctrica, Universidad de Oviedo, Spain (e-mail: jlaviada@tsc.uniovi.es, flasheras@tsc.uniovi.es).

Digital Object Identifier 10.1109/TAP.2017.xxx

redundant sampling techniques can be directly applied [15]. Once the phase of the AUT is retrieved, the far-field (FF) can be computed by employing conventional NF-FF transformation techniques. Also the fields in the aperture can be obtained for diagnostics purposes.

The rest of the paper is structured as follows. The scalar calibration technique is presented in Section II, together with a brief description of the broadband indirect off-axis holography method [and the error analysis](#). A numerical example is shown in Section III for a reflector antenna characterization in the W-band. Measurement results for the characterization of a double reflector, also in W-band, are shown in Section IV. Finally, main conclusions are drawn in the last section.

## II. METHOD

As mentioned above, this work extends our previous method in [14] to overcome the need of vector calibration and, thus, only the key points of the broadband off-axis holography will be presented here in order to ease the reading process.

### A. Broadband Off-axis Holography

The hologram, or interference pattern, formed with the fields coming from the AUT (or auxiliary antenna in the additional step) and the reference antenna is acquired for a set of frequencies at each point of the acquisition plane (see Fig. 1 for a description of the setup), and then, the broadband phaseless technique based on indirect off-axis holography computes the hologram point-by-point in the acquisition plane simultaneously for all the frequencies as

$$H(\vec{r}, \omega) = |E_{aut}(\vec{r}, \omega) + E_r(\vec{r}, \omega)|^2 = |E_{aut}(\vec{r}, \omega)|^2 + |E_r(\vec{r}, \omega)|^2 + E_{aut}(\vec{r}, \omega)E_r^*(\vec{r}, \omega) + E_{aut}^*(\vec{r}, \omega)E_r(\vec{r}, \omega), \quad (1)$$

where  $\vec{r}$  denotes the position of the probe in the acquisition plane,  $\omega$  is the angular frequency and  $E_{aut}$  and  $E_r$  are the fields of the AUT and the reference antenna, respectively. The asterisk represents the complex conjugate of the field.

If the amplitude of the AUT and the reference antenna are characterized independently, the so-called modified hologram can be computed as shown in (2) and, furthermore, the measured amplitude can be used with the retrieved phase, to improve the accuracy of the technique.

$$H_m(\vec{r}, \omega) = H(\vec{r}, \omega) - |E_{aut}(\vec{r}, \omega)|^2 - |E_r(\vec{r}, \omega)|^2 = E_{aut}(\vec{r}, \omega)E_r^*(\vec{r}, \omega) + E_{aut}^*(\vec{r}, \omega)E_r(\vec{r}, \omega) \quad (2)$$

The spectrum of the modified hologram in the time domain has two terms, known as image terms, and can be expressed as

$$h_m(\vec{r}, t) = e_{aut}(\vec{r}, t) \otimes e_r^*(\vec{r}, -t) + e_{aut}^*(\vec{r}, -t) \otimes e_r(\vec{r}, t), \quad (3)$$

where  $e_{aut}$  and  $e_r$  are the inverse Fourier Transform (FT) of  $E_{aut}$  and  $E_r$ , respectively, and  $\otimes$  denotes the convolution operator.

As can be seen, the first term corresponds to the convolution of the spectrum of the AUT and the conjugate of the spectrum of the reference antenna, and therefore contains information about the amplitude and phase of the AUT. This term can be filtered as shown in (4) by means of a rectangular window  $R(t_1, t_2)$ , defined from  $t_1$  to  $t_2$ ,

$$h_{m\_filt}(\vec{r}, t) = h_m(\vec{r}, t)R(t_1, t_2) \simeq e_{aut}(\vec{r}, t) \otimes e_r^*(\vec{r}, -t), \quad (4)$$

providing all the requirements described in [14] to avoid time overlap are fulfilled. Then, the complex field of the AUT can be retrieved back in the frequency domain after removing the effect of the interfering field for each point of the acquisition plane:

$$E_{aut}(\vec{r}, \omega) \simeq H_{m\_filt}(\vec{r}, \omega)/E_r^*(\vec{r}, \omega), \quad (5)$$

being  $H_{m\_filt}$  the FT of the filtered image term.

Fig. 1. Broadband off-axis holography measurement setup scheme.

It is worth noting that  $E_r^*(\vec{r}, \omega)$  is a term with low variability in the frequency domain and, consequently, there is no risk of divisions by zero in (5).

In the proposed method, the previous technique is applied twice. In the first step, the AUT is replaced by an auxiliary antenna, employed to retrieve the phase of the reference antenna in its final position of the setup, as shown in Fig. 1 (STEP 1); in the second step the retrieved field of the reference antenna is employed to retrieve the phase of the AUT (see Fig. 1 STEP 2). It is important to highlight that the first step has to be applied only once if the same reference antenna in the same position is employed for several antenna characterization.

### B. Scalar Calibration: Auxiliary Antenna Phase Modeling

As it can be seen in (5), to remove the effect of the interfering field, it is necessary to know its amplitude and phase. To complete the process only from scalar acquisitions, the complex field of the auxiliary antenna, an Open-Ended Waveguide (OEWG), is analytically modeled as:

$$E_{aux}(\vec{r}, \omega) = |E_{aux}(\vec{r}, \omega)|e^{-jk_0 \cdot (\vec{r} - \vec{r}_0)}e^{-j\beta_n l_n}, \quad (6)$$

where  $|E_{aux}|$  is the amplitude of the auxiliary antenna, which can be measured, and  $k_0$  is the wavenumber. The first exponential term models the spherical wave front propagating from the center of the auxiliary antenna aperture, defined by  $\vec{r}_0$ , to each point of the acquisition plane, and the second exponential term accounts for the propagation inside the antenna.  $\beta_n = 1/(c\sqrt{\omega^2 - \omega_c^2})$  is the propagation constant inside the OEWG with  $\omega_c$  being the cutoff angular frequency, and  $l_n$  the length of the OEWG.

An OEWG antenna is chosen for two reasons: 1) it is a simple antenna, with a theoretical model, and 2) in off-axis indirect holography the antenna used to create the interference is normally a non-directive antenna (i.e. OEWG and/or small horns) because they allow for a uniform illumination of the acquisition plane by means of their main lobe (spherical fronts) [6]. The use of other type of antennas with more directive diagrams would cause a dynamic range reduction, increasing the error of the phase retrieval. Furthermore, for NF acquisitions the existence of nulls in the acquisition plane, will yield erroneous results after NF-FF transformation [1].

The model in (6), approximates the behavior of the reference field with very low error, as shown in Fig. 2, where the phase of a 2 cm OEWG antenna (as the one employed in the numerical example) obtained with the simulation software Feko [18], is compared to the one obtained with the proposed model at 92.5 GHz, central frequency of the W-band. A maximum error of  $3.2^\circ$  is observed, disregarding some  $180^\circ$  phase shifts.

The error in the Euclidean norm of the phase model for the complete frequency band, computed as described in (9), is below 0.4% for all the frequencies, as depicted in Fig. 3, with a mean value of 0.11%. The slightly larger values in the upper part of the band can be attributed to the variation of the phase center position with

frequency, and, as it is shown in the validation example, it does not have a strong impact in the final results.

$$\text{error}[\%] = 100 \frac{\|\vec{E}_{\text{simulation}}(r, \omega) - \vec{E}_{\text{analytical}}(r, \omega)\|_2}{\|\vec{E}_{\text{simulation}}(r, \omega)\|_2} \quad (7)$$

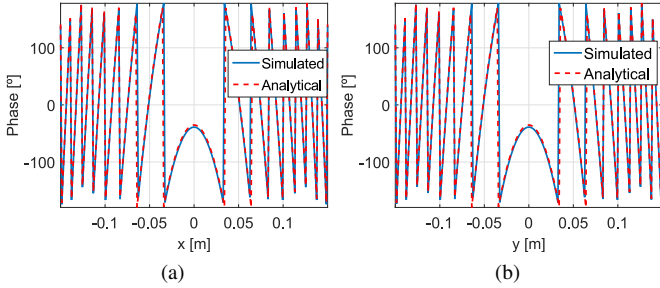


Fig. 2. Main cuts of the phase of the auxiliary antenna at 92.5 GHz in the acquisition plane. (a)  $x = 0$  cut, (b)  $y = 0$  cut.

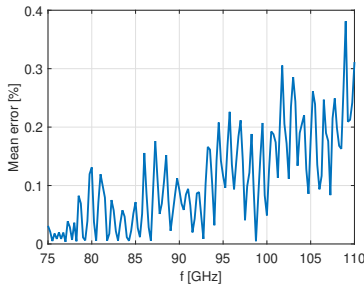


Fig. 3. Mean error of the phase retrieval for the numerical example.

### C. Error Analysis

The sources of error can be classified into two main groups: error due to the measurement system in the phase retrieval, and errors inherent to the calibration method caused by the analytical phase model and the auxiliary antenna position uncertainty.

The effect of noise and drift in the RF instrumentation as well as the mechanical errors has been analyzed in [6], [9] for conventional off-axis holography. In [15], the analysis is extended for the broadband phaseless method in [14] for a reduced set of acquisition points. While slightly more sensitive to noise and xy-positioning errors, off-axis indirect holography methods have proven to be more robust to planarity errors (z-axis) which are the dominant source of mechanical errors in planar scans [6], [15].

Regarding the proposed calibration method, it is relevant to observe first that the error due to the overlap between the different terms of the hologram given in (3) can be reduced to a negligible level by a proper design of the propagation delays [14]. Thus, it results that:

$$H_{m, \text{filt}}(\vec{r}, \omega) \approx E_{\text{aut}}(\vec{r}, \omega) E_r^*(\vec{r}, \omega). \quad (8)$$

The amplitude of the reference antenna can be easily measured in the phaseless measurement setup and, therefore, errors in the characterization of the reference antenna are expected to be in the phase term. Consequently, if (5) is applied with an error contaminated reference field,  $\hat{E}_r^*(\vec{r}, \omega)$ , then the retrieved field can be expressed as

$$E_{\text{ret}}(\vec{r}, \omega) \approx \frac{H_{m, \text{filt}}(\vec{r}, \omega)}{\hat{E}_r^*(\vec{r}, \omega)} = E_{\text{aut}}(\vec{r}, \omega) e^{j\Delta\varphi(\vec{r}, \omega)}, \quad (9)$$

where  $\Delta\varphi(\vec{r}, \omega)$  is the phase error between the real reference field and the modeled one. Therefore, each degree of error in the phase,

which can be due to a mismatch with the theoretical model or due to alignment, will directly translate into a degree of error in the retrieved field under the aforementioned conditions. This fact points out that the most critical point of the approach is a correct characterization of the auxiliary antenna as any error has a cumulative effect and will propagate to the near-field of the AUT.

### III. NUMERICAL VALIDATION EXAMPLE

The proposed method for scalar calibration of the reference antenna has been validated first by means of a numerical example. In particular, a measurement setup for the phase retrieval of a 30 cm diameter parabolic reflector with a  $\cos^q(\theta)$  feed ( $q = 1$ ) and 49.3 dBi directivity has been simulated.

The reference antenna is a 2 cm WR-10 OEWG identical to the auxiliary antenna, whose phase model is shown in Fig. 2. The reference antenna is placed at  $d_r = 17$  cm of the origin of coordinates  $O$ , with an off-axis angle of  $\theta_r = 15^\circ$ . A graphical description of the layout of the setup is depicted in Fig. 1.

The NF data are computed on a rectangular plane of 30 cm x 30 cm at  $z_0 = 45$  cm of the aperture of the AUT. The acquisition is made for 201 frequency points equally spaced from 75 to 110 GHz, covering the complete frequency band. Despite being a phaseless acquisition, the spatial sampling can be set to  $\lambda/2$  at the highest frequency of the band, that is 1.4 mm, owing to the fact that the phase retrieval is done point-by-point simultaneously for all the frequencies [14].

In both steps, the amplitude of the auxiliary and reference antennas and the AUT are independently acquired in order to compute the modified hologram and improve the quality of the phase retrieval.

#### A. Phase Retrieval

For the calibration step, the auxiliary antenna, a 2 cm OEWG antenna is placed at the origin of coordinates in the position of the AUT (see Fig. 1) and the broadband holography method [14] is applied to retrieve the phase of the reference antenna in its final position from the interference pattern created by the auxiliary and reference antennas.

The main cuts of the retrieved phase of the reference antenna are shown in Fig. 5 (a) and (b) compared to the reference cuts, obtained directly by simulation. Very good agreement is observed between the reference results and those obtained with the calibration method. Mean error in the complete band is computed as defined in (7) and shown in Fig. 4.

As justified in [14], the filtering process from which  $h_{m, \text{filt}}$  is obtained (4), implies windowing the part of the spectrum corresponding to  $e_{\text{aut}}(\vec{r}, t) \otimes e_{\text{ref}}^*(\vec{r}, t)$ . This time domain filtering will yield invalid values in the extremes of the frequency band once the filtered signal is transformed back to the frequency domain into  $H_{m, \text{filt}}$ , and thus, it is necessary to discard the lower and higher parts of the frequency band. Fig. 4 shows the error behavior in the complete band for the phase retrieval of the reference antenna. The working band has been selected from 80 GHz to 105 GHz, which, for this numerical example has a maximum error of 2% and a mean value of 0.11%. The proposed method has proven to provide accurate pattern results even when the mean error level is close to 10% as it will be seen in the measurement example.

The main cuts of the retrieved phase of the reference antenna are shown in Fig. 5 (a) and (b) compared to the reference cuts, obtained directly by simulation for the central frequency. Once the phase of the reference antenna is known, the AUT is installed in the same position of the auxiliary antenna and the broadband holography method is applied a second time to retrieve the phase of the AUT. As shown with a dashed red trace in Fig. 4, mean error is slightly increased to 0.84% in the working band, which translates into a small ripple

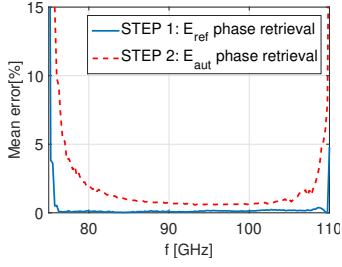


Fig. 4. Phase retrieval mean error for both steps for the numerical example.

with a peak-to-peak variation of  $1.79^\circ$  in the  $y$ -axis and  $2.73^\circ$  in the  $x$ -axis of the retrieved phase of the AUT as shown in Fig. 5 (c)-(d).

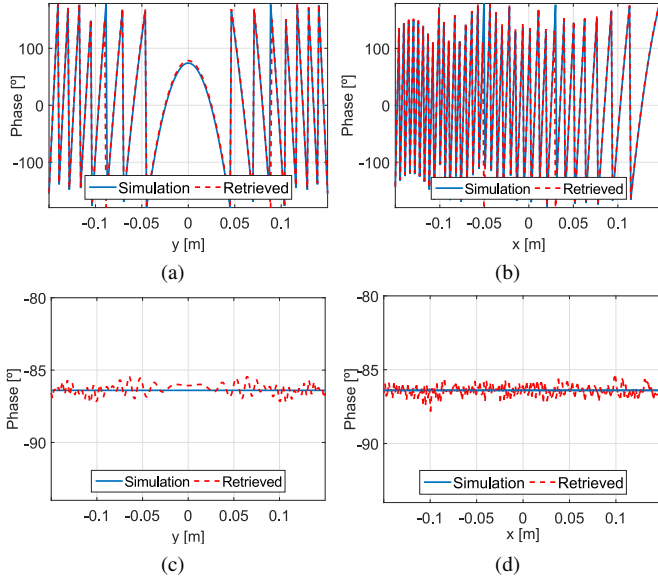


Fig. 5. Main cuts of the retrieved phase of the reference antenna and AUT at 92.5 GHz. (a) Reference antenna  $x = 0$  cut, (b) Reference antenna  $y = 0$  cut. (c) AUT  $x = 0$  cut, (d) AUT antenna  $y = 0$  cut.

The higher value of the error in the second step is due to the cumulative effect of the error. Nevertheless, as shown in the next section, the achieved accuracy is good compared to other phaseless-techniques [6], [7], [12] and this small error in the phase retrieval has not a very large impact in the computed FF of the AUT.

### B. Far-field Pattern Computation

Once the amplitude and phase of the AUT are known, conventional NF-FF transformation methods can be applied to obtain the radiation pattern of the AUT. In this case, the implemented NF-FF is based in the plane wave expansion method [1]. The main cuts of the radiation pattern for the central frequency of the band are shown in Fig. 6 compared to the reference results obtained directly from simulations. The agreement between the reference results and those obtained with the proposed method is high, as proven by the low level of the difference plot, below  $-70$  dB, except for the secondary lobes in the  $\phi = 0^\circ$  cut close to  $-60$  dB.

The computed directivity of the pattern obtained from phaseless measurements is  $49.31$  dBi, only  $0.01$  dB higher than the value obtained from simulations, validating the proposed calibration technique.

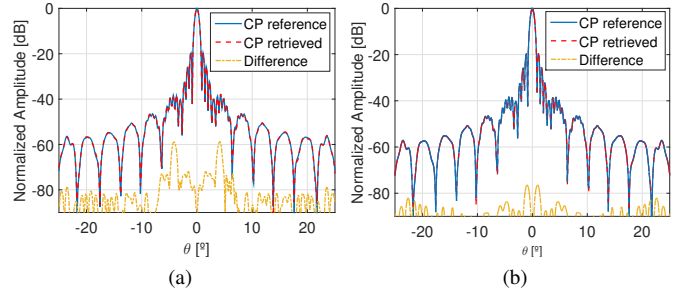


Fig. 6. Radiation pattern main cuts at 92.5 GHz. (a)  $\phi = 0^\circ$ , (b)  $\phi = 90^\circ$ .

## IV. MEASUREMENT EXAMPLE

A similar setup to the one employed for the numerical example has been implemented for the measurement validation. In this case, an *ad-hoc* double reflector antenna has been designed to model a directive antenna (directivity  $\geq 50$  dBi). The main reflector is a  $30$  cm diameter parabolic dish and the secondary reflector is a  $4.8$  cm diameter planar reflector, placed  $13$  cm above the vertex of the main reflector, considered the origin of coordinates (see Fig. 7(b)). The feed is a  $10$  cm WR-10 OEWG, implemented by means of two straight waveguide sections of  $5$  cm, whose aperture is positioned  $11$  cm above the origin of coordinates and will also be employed as the auxiliary antenna.

The reference antenna is a  $3$  cm tapered-end OEWG antenna. The antenna is placed pointing to the center of the acquisition plane with an off-axis angle of  $15^\circ$  and with the center of its aperture in  $(x_r, y_r, z_r) = (0, 17, 4.2)$  cm. A  $30$  cm flexible cable with WR-10 flanges at both ends is employed to connect the reference antenna with the  $-10$  dB output port of a directional coupler. Both the cable and the effect of the coupler will be considered in the proposed calibration method.

A 3D-printed support has been designed in order to fix the position and off-axis angle of the reference antenna and the AUT (and auxiliary antenna) as can be seen in Fig. 7.

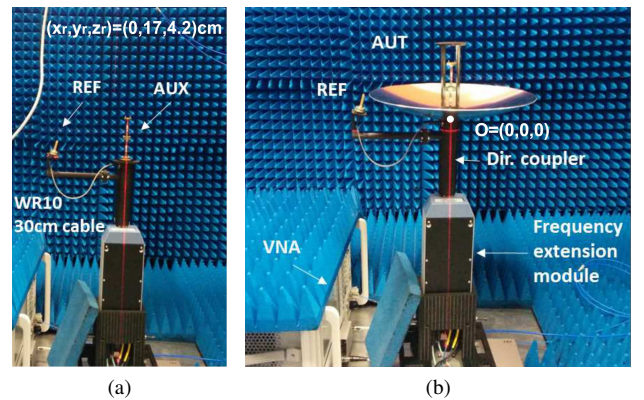


Fig. 7. Measurement setup. (a) STEP 1: Reference antenna phase retrieval with auxiliary antenna, (b) STEP 2: AUT phase retrieval.

The acquisition plane is a  $50 \times 50$  cm plane at  $z_0 = 39.9$  cm, yielding a valid margin for the NF-FF transformation of  $14^\circ$  [1]. Spatial sampling, has been set to  $\lambda/2$  at  $110$  GHz, as in the simulation example, and  $201$  equally spaced frequency points, from  $75$  GHz to  $110$  GHz, are recorded at each point of the spatial acquisition.

Additionally, direct complex field acquisitions (amplitude and phase) of the AUT, auxiliary and reference antennas have been performed as reference measurement to compare to the results of the

proposed method. A comparison between the uncertainties caused by the main sources of error in the computation of the antenna pattern for complex acquisitions and broadband phaseless acquisitions has been presented in [15].

### A. Phase Retrieval

First step, as in the previous case, is to compute the phase model of the auxiliary antenna. As above mentioned, the auxiliary antenna is composed of two 5 cm sections of WR-10 waveguides. Thus, the antenna is modeled by means of (6) considering  $l_n = 10$  cm. The main cuts of the modeled phase are plotted in Fig. 8 compared to the real measurements at the central frequency of the band. As can be seen, the phase obtained with the proposed model is an accurate approximation for this type of antennas. Nevertheless, a small ripple can be observed in the central part of the measurements, being more noticeable in the cut for  $y = 0$  (see detailed view in Fig. 8(b)). This ripple is attributed to internal reflections inside the antenna, probably due to the use of two different waveguide sections, and cannot be filtered, increasing the error in the phase model. The average error for the phase model in the complete frequency band as defined in (9) is depicted in Fig. 9, its mean value is 0.53%.

As it has been observed in the numerical example, error has a cumulative effect through all the different steps and, thus, the 0.53% error in the phase model will increase the error level in the phase retrieval, when compared to those values obtained in the numerical example. However, error level is expected to decrease in the case of implementing the auxiliary antenna with only one waveguide section yielding also a substantial decrease of the error level of both phase retrieval steps.

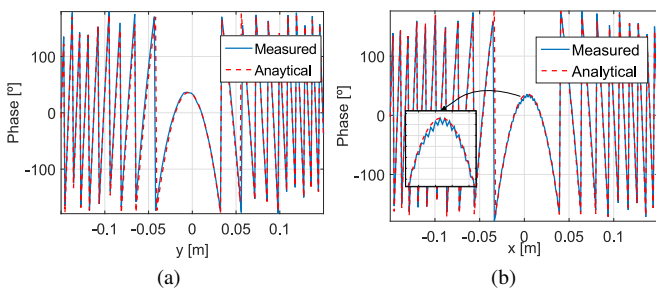


Fig. 8. Main cuts of the phase of the auxiliary antenna at 92.5 GHz in the acquisition plane. (a)  $x = 0$  cut, (b)  $y = 0$  cut.

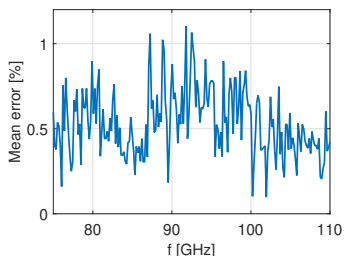


Fig. 9. Mean error of the phase model of the auxiliary antenna in the measurement example.

In an analogous way to the numerical example, next step is the phase retrieval of the reference antenna after acquiring the interference pattern of the reference and auxiliary antennas (see Fig. 7(a)). The obtained results for the central frequency of the band are shown in Fig. 10 (a) and (b) for the phase retrieval of the reference antenna. Apart from some  $180^\circ$  phase shifts in the main beam, the agreement between direct acquisitions and the retrieved phase from the scalar

calibration method is high with a maximum discrepancy of  $4.26^\circ$ . The error, computed from (7) is depicted in Fig. 11 in a blue trace for the first step of the proposed method. Its mean value is 0.25% in the complete frequency band and 0.18% in the working band.

Once the field of the reference antenna is known in amplitude and phase, the auxiliary antenna is replaced by the AUT, see Fig. 7 (b) for further details. The phase retrieval results are shown in Fig. 10 (c) and (d) for the main cuts of the AUT at the central frequency of the band, while the error in the complete frequency band is plot with a red trace in Fig. 11. Despite having a higher error than for the previous step ( 4.69% in the working band), the observed agreement between measurements and the retrieved phase is still fair.

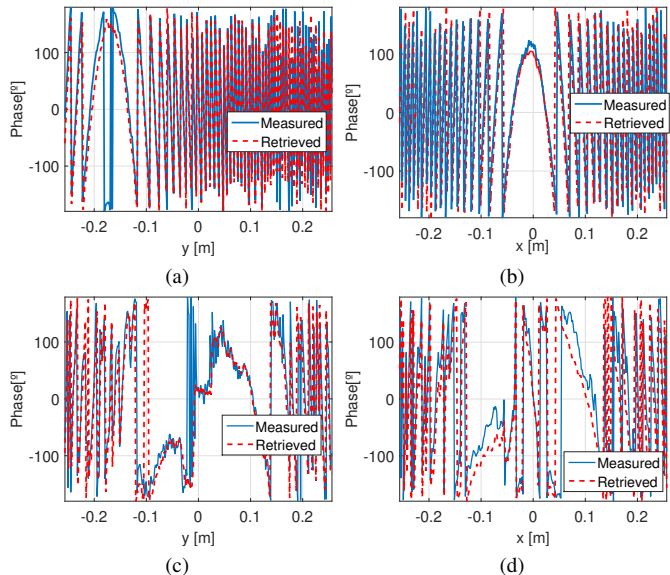


Fig. 10. Main cuts of the retrieved phase of the reference antenna and AUT at 92.5 GHz. (a) Reference antenna  $x = 0$  cut, (b) Reference antenna  $y = 0$  cut. (c) AUT  $x = 0$  cut, (d) AUT  $y = 0$  cut.

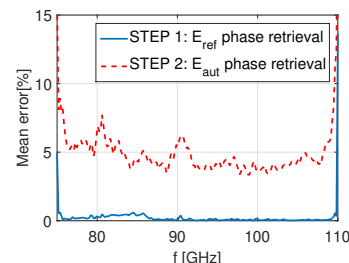


Fig. 11. Mean error of the phase retrieval for the measurement example.

The filtering process of the hologram in the time-domain, inherent to the phase retrieval process, has an equivalent effect than a conventional time-gating (which requires complex field knowledge). This effect is noticeable in the smooth retrieved phase of the AUT shown in Fig. 10 (c) and (d). This is indeed a big advantage, particularly useful in acquisitions affected by strong reflections or performed in non-perfect anechoic environments, as is this case here.

### B. Far-field Pattern Computation

Finally, the FF is computed from the measured amplitude and the retrieved phase of the AUT and compared to that obtained from NFF transformation of the direct acquisition of the field of the AUT with amplitude and phase. The main cuts of the FF pattern are shown in Fig. 12 at 80.6 GHz which, with a 7.76% of error in the phase retrieval of the AUT (see Fig. 9), represents the worst case scenario.

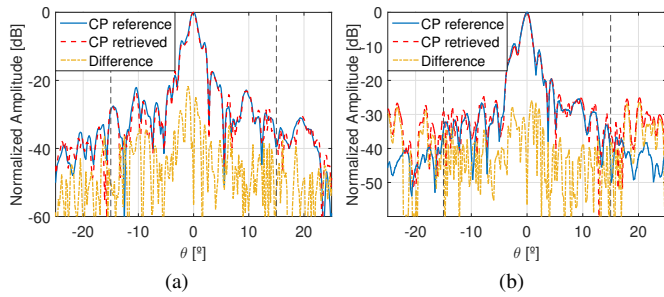


Fig. 12. Radiation pattern main cuts at 80.6 GHz. (a)  $\phi = 0^\circ$ , (b)  $\phi = 90^\circ$ . Vertical grey dashed lines define the valid angular margin of the NF-FF transformation.

A fair agreement is obtained inside the valid FF region ( $-14^\circ < \theta < 14^\circ$ ) despite the errors in the phase retrieval. The mean value of the FF error, calculated as the difference between the reference and the retrieved field, is approximately  $-52$  dB although it reaches  $-22$  dB in the main lobe. Nevertheless, the error in the directivity computation remains low, being  $39.51$  dBi and  $38.63$  dBi the reference and computed value from the phaseless acquisition, respectively.

## V. CONCLUSION

A scalar calibration method for phaseless broadband off-axis holography is presented. The method considers an additional step in which an open-ended waveguide antenna is employed as an auxiliary antenna to retrieve the phase of the reference antenna in its final position in the setup, being the effect of all the components of the setup (directional coupler and cables, waveguides, etc.) considered. The phase of the auxiliary antenna is analytically modeled and thus, the need of vector calibration is bypassed. By retrieving the phase of the reference antenna in its final position in the setup, the errors, inherent to the reference field characterization in indirect off-axis holography setups, are reduced. Once the reference field is known in amplitude and phase, the auxiliary antenna is replaced by the antenna under test and the broadband off-axis holography technique is applied a second time to retrieve the phase of the AUT.

The method can be applied to near- and far-field acquisitions and, since the phase is retrieved point-by-point in both steps, the proposed scalar calibration is compatible with non-redundant sampling techniques, allowing for a reduction of the acquisition time [15].

Another remarkable advantage with respect to monochromatic phaseless techniques is that the phase is retrieved coherently in the complete frequency band, therefore, the technique has the potential to perform group delay computations, very relevant for broadband antennas and high-rate communications. In contrast to iterative phase retrieval techniques, the method does not depend on the variability of the near-field, being specially well-suited for high-gain antenna characterization. Furthermore, similar effects to those obtained when applying time-gating techniques (requiring complex data) are achieved with the proposed method, being specially useful when working in non-anechoic environments.

The most crucial point of the proposed approach is the modeling of the phase of the auxiliary antenna as its error will propagate towards the phase retrieval of the AUT. Although this modeling is challenging, especially at high frequencies, in return, the proposed technique enables a very flexible off-axis approach with the possibility of changing the reference antenna position without the need of a vector calibration.

The proposed scalar calibration has been validated by means of simulations and measurements in the W-band considering single and

double reflector antennas, respectively. A good agreement is observed between the radiation patterns obtained with the proposed calibration method from amplitude-only acquisitions and the reference pattern in the numerical example achieving a peak error below  $-60$  dB. In measurements, the error is increased due to the inaccuracies of the phase model being its peak value approximately  $-20$  dB. However, these inaccuracies are attributed to inner reflections in the measurements, due to the fact that two sections of waveguides were used to implement the auxiliary antenna. Despite the increased error, the agreement of the radiation pattern obtained with the proposed scalar method is good compared to the measurements obtained from direct phase acquisition, proving the validity of the technique.

## REFERENCES

- [1] A. Yaghjian, "An overview of near-field antenna measurements," *IEEE Trans. Antennas and Propag.*, vol. 34, no. 1, pp. 30–45, Jan. 1986.
- [2] D. Gabor, "Microscopy by reconstructed wave-fronts," *Proc. of the Royal Soc. of London A: Math., Physical and Eng. Sci.*, vol. 197, no. 1051, pp. 454–487, Jul. 1949.
- [3] E. Leith and J. Upatnieks, "Reconstructed wavefronts and communication theory," *J. Opt. Soc. Amer.*, vol. 52, pp. 1123–1128, 1962.
- [4] P. Napier and R. Bates, "Antenna aperture distributions from holographic type of radiation-pattern measurement," *Proc. of the Institution of Electrical Eng.*, vol. 120, no. 1, pp. 30–34, Jan. 1973.
- [5] J. Bennett, A. Anderson, P. McInnes, and A. Whitaker, "Microwave holographic metrology of large reflector antennas," *IEEE Trans. Antennas and Propag.*, vol. 24, no. 3, pp. 295–303, May 1976.
- [6] G. Junkin, T. Huang, and J. Bennett, "Holographic testing of terahertz antennas," *IEEE Trans. Antennas and Propag.*, vol. 48, no. 3, pp. 409–417, Mar. 2000.
- [7] V. Schejbal, V. Kovarik, and D. Cermak, "Synthesized-reference-wave holography for determining antenna radiation characteristics," *IEEE Antennas and Propag. Mag.*, vol. 50, no. 5, pp. 71–83, Oct. 2008.
- [8] J. Laviada, A. Arboleya-Arboleya, Y. Álvarez-Lopez, C. García-Gonzalez, and F. Las-Heras, "Phaseless antenna diagnostics based on off-axis holography with synthetic reference wave," *IEEE Antennas and Wireless Propag. Lett.*, vol. 13, pp. 43–46, 2014.
- [9] A. Tennant, G. Junkin, and A. P. Anderson, "Relaxation of mechanical tolerances in phase retrieval antenna metrology," in *1993. 23rd European Microw. Conf. (EuMC)*, Sept. 1993, pp. 877–879.
- [10] A. Arboleya, J. Ala-Laurinaho, J. Laviada, Y. Alvarez, F. Las-Heras, and A. Räisänen, "Millimeter-wave phaseless antenna measurement based on a modified off-axis holography setup," *Journal of IR, Mm, and THz Waves*, vol. 37, no. 2, pp. 160–174, Feb 2016.
- [11] F. Las-Heras and T. Sarkar, "A direct optimization approach for source reconstruction and NF-FF transformation using amplitude-only data," *IEEE Trans. Antennas and Propag.*, vol. 50, no. 4, pp. 500–510, Apr. 2002.
- [12] Y. Álvarez, F. Las-Heras, and M. R. Pino, "The sources reconstruction method for amplitude-only field measurements," *IEEE Trans. Antennas and Propag.*, vol. 58, no. 8, pp. 2776–2781, Aug. 2010.
- [13] Y. R.-S. S.F. Razavi, "Phaseless measurements over nonrectangular planar near-field systems without probe corotation," *IEEE Trans. Antennas and Propag.*, vol. 61, no. 1, pp. 143–152, Jan. 2013.
- [14] A. Arboleya, J. Laviada, J. Ala-Laurinaho, Y. Alvarez, F. Las-Heras, and A. V. Räisänen, "Phaseless characterization of broadband antennas," *IEEE Trans. Antennas and Propag.*, vol. 64, no. 2, pp. 484–495, Feb 2016.
- [15] A. Arboleya, J. Laviada, J. Ala-Laurinaho, Y. Álvarez, F. Las-Heras, and A. V. Räisänen, "Reduced set of points in phaseless broadband near-field antenna measurement: Effects of noise and mechanical errors," in *2016 10th European Conf. on Antennas and Propag. (EuCAP)*, April 2016, pp. 1–5.
- [16] A. Tamminen, J. Ala-Laurinaho, and A. Räisänen, "Indirect holographic imaging at 310 GHz," in *2008. European Radar Conf. (EuRAD)*, Oct. 2008, pp. 168–171.
- [17] J. Laviada and F. Las-Heras, "Scalar calibration for broadband synthetic aperture radar operating with amplitude-only data," *IEEE Antennas and Wireless Propag. Lett.*, vol. 14, pp. 1714–1717, 2015.
- [18] "FEKO Suite 6.2 features. Last visited: 2016-07-12." [Online]. Available: <https://www.feko.info>